Springer

KSME

Journal of Mechanical Science and Technology 24 (2) (2010) 559~568
www.springerlink.com/content/1738-494x
DOI 10.1007/s12206-009-1222-6

Spray formation by a swirl spray jet in low speed cross-flow †

Sangseung Lee[1], Wonho Kim[2] and Woongsup Yoon[2,*]
[1]*Department of Weapons and Mechanical Engineering, Korea Military Academy, Gongneung-dong 77, Nowon-gu, Seoul, 139-799, South Korea*
[2]*Propulsion and Environmental Thermo-Fluid Laboratory, Department of Mechanical Engineering, University of Yonsei, Shinchon-dong 134, Seodaemun-gu, 120-749, Seoul, South Korea*

(Manuscript Received June 18, 2009; Revised August 24, 2009; Accepted September 23, 2009)

Abstract

Breakup and spray formation of swirl liquid jets introduced into a low-speed cross-flow are experimentally investigated. Effects of the cross-flows on the macro and microscopic spray parameters are optically measured in terms of jet Weber number and liquid-to-gas momentum ratio. At lower jet Weber numbers, the liquid stream undergoes Rayleigh jet breakup. At higher momentum ratios, bag breakup occurs and tends to distort the liquid column into a loop-like structure. As the jet Weber number rises, stronger aerodynamic interaction and secondary flows cause multi-mode breakup. Regardless of the momentum ratio, the spray profile is hardly altered at higher jet Weber numbers. The cross-flow promotes the jet breakup and renders a finer spray in an entire range of injection velocities.

Keywords: Cross-flows; Liquid jet weber number; Momentum ratio; Swirl liquid jet

1. Introduction

In many industrial applications, sprays are introduced into a cross-flow of non-zero relative velocity. Due to promoted transports of mass, momentum, and energy between the liquid and gas streams, strong momentum and wave energy carried by the gas stream exerts additional aerodynamic force on the liquids. Aerodynamic interaction overwhelms the surface tension, activates the deviation from the liquid-to-gas interface, and amplifies unstable waves, which causes a prompt atomization of the liquid jet. Enhancement of the microscopic spray characteristic is achieved. Application of this convection-assisted spray formation is diverse in the industry, including fuel injection in turbo-jet, ramjet, scramjet combustors [1-7] and urea injection for NO_x of the diesel exhaust [8]. In these applications, inflows are naturally induced by breathing or exhausting the gas and thus secure higher atomization quality with no additional cost.

Experimental studies on the penetration and the breakup of the liquid jets injected normal to high-Mach subsonic air-streams through injection ports of various geometries and sizes are bulky and the correlations of the jet penetration to essential injection parameters have been suggested [1]. Spray appearance, penetration height, velocity field, and liquid property were also investigated [1-5]. Both sub- and supersonic cross-flows were examined. Instant shadowgraph pictures showed that the liquid column breakup resembles the secondary breakup of a spherical droplet flying in a stagnant gas [3]. The jet column breakup was also addressed in terms of the of the wave parameters [2]. The surface waves of large amplitude propagating on the liquid jet at a sizable velocity of an order of the injection velocity command the jet integration. Microscopic spray structure including cross-sectional diameter distribution, centerline properties, and flux-averaged properties were reported with correlations [4]. Secondary breakup of droplets through shock wave interaction was also investigated. Serial pictures of droplet perturbed by the shock wave interaction revealed that a spherical droplet is deformed by the aerodynamic forces and then disintegrates sequentially while it experiences bag, multimode (bag/plume), and plume/shear breakup mode as the jet Weber number rises [9]. Primary breakup of a round non-turbulent liquid jet introduced into the gaseous cross-flows was visually shown using pulsed shadowgraph and holograph technique.

Qualitative similarity between the liquid column breakup in cross-flows and the aerodynamic secondary breakup of a spherical droplet was repeatedly but analytically shown by Wu et al. [7]. Fuller et al. [5] extended this method and examined effects of injection angle. Parametric studies on the spray characteristics yield better understanding of the spray dynamics as well as a database essential to the spray control technology. Jet breakup, liquid column trajectories and distance to column fracture points were measured in terms of injection liquids, injector diameters, and cross-flow Mach numbers [3-

† This paper was recommended for publication in revised form by Associate Editor Gihun Son

*Corresponding author. Tel.: +82 2 2123 4812, Fax.: +82 2 312 2159
E-mail address: wsyoon@yonsei.ac.kr

5]. Experimental and analytical studies in order to find practical correlations have been made. Taylor [10] theoretically solved a potential flow in a swirl injector and provided a linear relation of the film thickness and spray angle. Rizk and Lefebvre [11, 12] extended this linear method and conducted theoretical and experimental studies on the internal and external spray characteristics. A parametric examination of the film thickness, breakup length and spray cone angle was made in conjunction with the flow condition and the geometry [13-15]. Experiments of the near field of the swirl sprays were also made [16].

These early studies generally centered on elucidating the spray formation by a plain liquid jet injected from a single circular or non-circular orifice. The plain injector incorporated with a single orifice element highly fulfills essential injector requirements such as manufacturability and controllability. But the single-orifice injection method is not particularly appropriate for generating a finer spray because high injection pressure prerequisite to the generation of the finer spray is frequently badly fit for the system requirement or costly. Among various atomizing patterns, a pressure swirl spray provides a cost-effective substitute. Usefulness of pressure swirl jets has been demonstrated in diverse applications such as numerous industrial furnaces, liquid-propellant rocket engines, and ramjet and scramjet engines. In particular, two of aforementioned applications, the ramjet and scramjet combustor, employ the swirl jets situated in crossing air flows. Typically, a stringent requirement for these high-thrust super and hypersonic air-breathing engines is highly fulfilled by the swirl injection method because of its massive supply of the liquid fuel and minimum pressure loss.

In the present study, breakup and spray formation of the swirl liquid jet introduced into strongly convective cross flows is experimentally investigated. Effects of the cross-flows on the transients of jet breakup, atomization, and spray formation are visually discussed. Structure and characteristics of the spray including drop size, cross-sectional distribution of the drop size, penetration height and breakup length are optically measured. Interactions between the liquid jet and the cross-flow and resultant spray formation are discussed in terms of Weber number and momentum ratio.

2. Formation of the swirl spray

The pressure swirl atomizer is featured by additional breakup mechanism (swirling) for disintegration and atomization of the liquid. It converts the total pressure into angular momentum as the liquid passes through the helical path within the swirl chamber. Because of the centrifugal force due to the swirling motion of the liquid film on the swirl chamber, the conical liquid sheet exiting the injection orifice expands in the radial direction as it projects into downstream, and grows progressively thinner for continuity. Promoted by higher number density and higher relative velocities of the drops, droplet collision is expected to be a frequent event immediately after

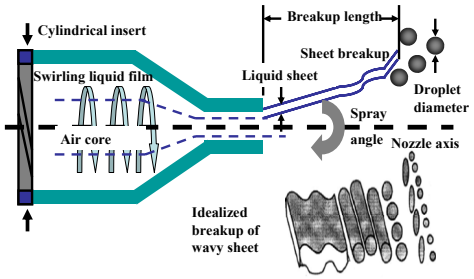

(a) Swirl injection element and spray formation

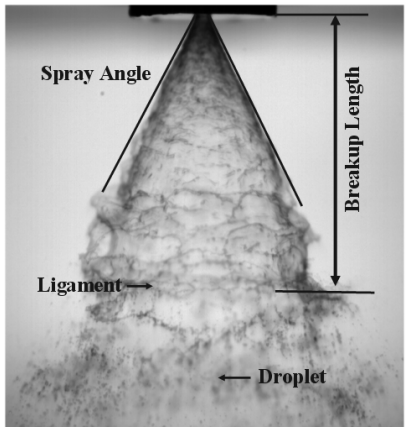

(b) Breakup of swirl liquid jet

Fig. 1. Illustration of swirl injection element and instant spray formation by swirl element (with no cross-flows).

the sheet breakup. The centrifugal force due to swirling motion causes an occurrence of the hollow-conical sheet anchored at the injection nozzle exit. Thin hollow-cone liquid sheets result in the formation of finer spray and narrow spectrum of the drop size.

Fig. 1(a) and (b) illustrate the formation of the pressure swirl spray and its instant profile, respectively. The liquid fed into the swirl chamber is forced to follow a helical path within the swirl chamber and then emerges from the nozzle in the form of a hollow conical sheet so that soon unstable waves develop and liquid disintegration occurs. As a result, the liquids are crowned along the conical skirt but void in the vicinity of the spray axis.

A large-scale mechanical mixing of the liquids is attained by multiple injection elements, and the well designed pressure swirl element gives rise to high atomization quality. In Fig. 1 (b), a photograph of the evolving spray shows that the liquid sheet breaks up and evolves intermittently into drops after the injection. Thereinafter, the initial spray propagates, disperses or shatters into smaller drops.

3. Experimental setup and test conditions

Fig. 2 illustrates a test setup consisting of sections of pressurization, regulation, test, optical imaging and data acquisition. The test section is installed with a small-scale subsonic wind tunnel in which the cross-flow flows and interacts with swirl

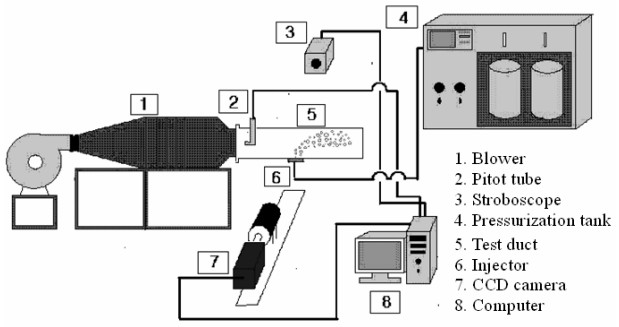

Fig. 2. Schematic of the spray test facilities.

liquid jet. A PC-based data acquisition system controls and records pressure and mass flow rate. The mass flow rate is precisely maintained by advanced servo circuits in order to limit the fluctuation of pilot tank pressure.

Air is blown into the subsonic wind tunnel equipped with a test sector of a rectangular cross-section (150mm×150mm) with its inflowing speed in the range of 10 and 40 meters per second. A pulsed shadow-graph technique was used to capture instant images of the spray. CCD (charge-coupled device) camera (Flow-Master 3S, LaVision Inc.) is synchronized with an illumination by a stroboscope. PTU (programmable timing unit) commands this sequence and limits the exposure duration within 15 nano seconds. A Questar QM100 (Questar Corp.) long focal microscope lens was used for capturing instant images of higher resolution. Image capturing unit is saddled on a traversing rail. After taking 50 consecutive snapshot pictures, it shifts to the next coordinate and places the focal point of the high-power object lens onto a predetermined lattice point. Every image is stored for analysis once the imaging is completed. Two spherical particles of the mist droplet (3μm) and the steel ball (500μm) were imaged and measured to find the reduction ratio. 3μm droplet was captured from the mist generated by the humidifier. Generally, the mist drops due to the humidifying electric vibration are highly monodisperse and the drop size distribution is considerably narrow-banded in the vicinity of 3μm.

To distinguish the presence of the droplet and measure the drop size, all images are scanned for the pixels, and crude pixel data are filtered in advance in order to eliminate the noise. The imaging areas of the sampling point are 3mm times 2.4mm in still atmosphere and 3.4mm times 2.7mm in cross-flows with each other. When the number density of the pixels is greater than the threshold value, that space is regarded as the liquid, or the gas (vapor). Once the liquid volume is recognized, its aspect ratio is calculated. The image processing problem in the pulsed shadow-graph technique using a stroboscope and micro-lens that droplet images in the rear region of the spray may be partly sometimes totally blocked by droplets located in the front region of the spray can be solved by recognizing the droplets on focusing them for the sampling point. In addition, other problems in image processing related to droplets extending over the sampling window or coalescence of them due to collision can be solved because the liquid volume of the aspect ratio in the range from 0.8 to 1.2 is counted as droplet. An arithmetic mean diameter of individual droplets is obtained and stored for the SMD calculation. To ensure highly-resolved spray data with 95% confidence limits, 5,000 drops were sampled for the SMD calculation [17].

Table 1. Geometric and operational parameters of pressure swirl injector.

Swirl chamber diameter	2.5 mm	Injection pressure	0.0355-0.7 MPa
Swirl chamber length	12 mm	Injection rate	1.4-9.6 g/s
Orifice exit diameter, d	1 mm	Gas velocity	6-40m/s
Injection Orifice length, L	1.5 mm	Re_l	3,800-25,300
Entry slot	4	We_l	0.25-10.89
Discharge coefficient	0.28-0.33	Momentum Ratio, q	9-3,300

* Re_l : Reynolds number of injected liquid jet
We_l : Weber number of injected liquid jet with regard to the cross-flow velocity

A detailed understanding of the spray dynamics in conjunction with cross-flows is the principal aim of the present study. To this end, parameters commanding atomization of liquid jets are bound into suitable ranges. Essential geometric and operational parameters are summarized in Table 1.

Injection rate of the water is in the range from 1.4 to 9.8 g/s (injection velocities from 3.9 to 25.4m/s) due to LISA method (linear instability sheet atomization) [18-19] or, equivalently, jet Reynolds number ($Re_l \equiv \rho V_l d_0 / \mu$) approximately from 3,800 to 25,300. Here V_l and d are the injection velocity and the orifice diameter, respectively. Ranges of the jet Weber number and the liquid-to-gas momentum ratio in Table 1 were readily obtained from the gas and liquid jet velocities.

Characteristics of a plain single-orifice spray introduced into a subsonic cross-flow largely depend on the cross-flow velocity rather than transport properties of the liquid [6, 7]. Accordingly, the spray characteristics may be better addressed in terms of the flow properties rather than the fluid properties. For cross-flows, the inflowing air speed was varied in the range from 6 to 40 m/s, or equivalently, the Reynolds number of the gas in the range from 400 to 2,800. The air stream from a blower may be turbulent or concurrent with complicated secondary flows such as cascading flow recirculation. The air flow introduced into the duct is laminarized while it passes through a honeycomb stabilizer installed immediately downstream of the blower, hence the air-flow is laminar and carries axial momentum only. Pitot-tube tests conducted at the exit of the honeycomb stabilizer verified the occurrence of uniform cross-sectional velocity distribution with minimal spatial variations.

Interrupted by strongly convective cross-flows, the drops (or the spray) quickly decelerate by the aerodynamic drag, settle down to the gas flow, and evolve into a drop-laden flow downstream. Neglecting the gravitational acceleration, terminal velocity of a droplet situated in the traversing gas stream is set to be

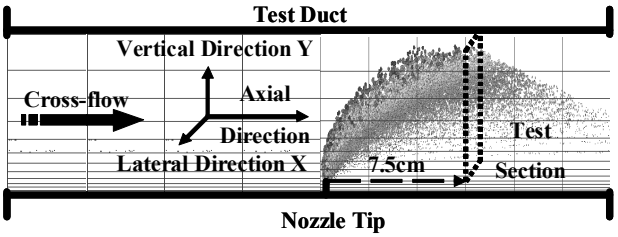

Fig. 3. Schematic of swirl spray formation in the cross-flows (13×13 sampling points on the cross-section at the axial distance 7.5 cm from the nozzle tip).

equal to that of the gas flow. A stopping time (an interval during a stagnant droplet is accelerated up to the gas velocity) is proportional to square of the droplet diameter. In the practical size range, the droplet promptly adjusts to the gas motion. At standard conditions, the stopping time for a droplet of 100 μm diameter in the cross flow of the relative velocity of 10 m/s is on the order of 10^{-2} second.

Fig. 3 illustrates the profile of the test duct. The aerodynamic interaction caused by non-zero relative velocity is activated in a narrow region centered on the liquid stream, and the atomization including the secondary breakup rapidly diminishes as the spray proceeds downstream. Thus, the axial location for imaging and measuring the spray could be safely chosen as 7.5 cm down the stream from the nozzle tip in cross-flows. It is noted that the swirl jet was injected downward when the cross-flow velocity was zero in order to prevent the gravitational bending of the spray. Measurement was made on the cross-section located at 4 cm downward from the nozzle tip.

4. Results and discussion

The atomization quality was examined in terms of Weber number of the liquid jet and the liquid-to-gas momentum ratio.

Generally speaking, the jet Weber number ($We_l \equiv \rho_g d (u_l - u_g)^2 / \sigma$) in high speed cross-flows is defined as the ratio of the momentum flux of the gas flow acting onto the liquid to surface tension restraining the liquid. This is because, with no presence of interrupting gas flows, the degree of atomization is a function of the ratio of a relative magnitude of activation (liquid jet momentum) to that of attenuation (surface tension).

On the other hand, in the event of a spray formation in traversing gas flows, vertical momentum carried by the liquid jet commands the gas-liquid interaction because the gas flow traverses the liquid jet but its extent just ends over the jet diameter and its vertical component is minimal. Conclusively, the relative velocity between the gas and liquid streams for the jet breakup is very proximate to, hence replaced by, the vertical injection velocity of the liquid jet [20].

Inertial effect of the cross-flow on the liquid jet breakup is estimated in terms of the momentum ratio ($q = \rho_l u_l^2 / \rho_g u_g^2$), which is defined as the ratio of the liquid jet momentum to that of the cross-flow and hence measures the relative inertial strength of the liquid jet.

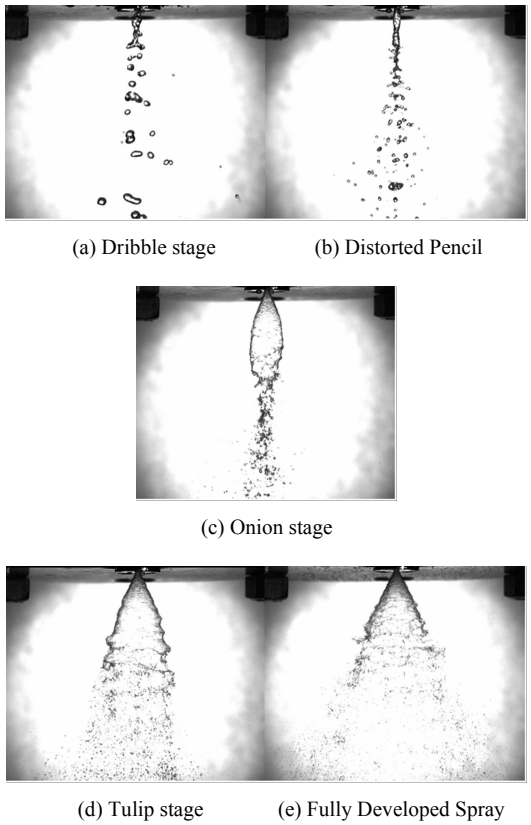

(a) Dribble stage (b) Distorted Pencil

(c) Onion stage

(d) Tulip stage (e) Fully Developed Spray

Fig. 4. Transition of spray patterns due to change in the jet Weber number (We_l) (due to increasing injection pressure): (a) 203 (b) 371 (c) 657 (d) 2,020 (e) 8,834.

At higher jet Weber numbers, the hollow liquid cone grows wider due to augmented centrifugal force and becomes progressively thinner for continuity as it proceeds downstream. Concurrent with evolution into thinner liquid sheet, perforation breakup mode occurs. This breakup process is relevant to the local point disturbance originating from the turbulence and promotes ligament formation. That is, the momentum exchange between liquid jet and cross-flow is predominant. The opposite holds for an injection at lower jet Weber number, and thus the atomization quality depends on the liquid-to-gas momentum ratio.

Hereinafter, the dynamics and characteristics of the spray are addressed in terms of the jet Weber number and the liquid-to-gas momentum ratio (briefly Weber number and momentum ratio hereinafter).

4.1 Breakup and spray formation in still atmosphere

In a pressure swirl atomizer, liquids are injected through tangential or helical passage into a swirl chamber from which it emerges with both tangential and axial velocity components to form a thin conical sheet at the exit. A centrifugal force originating from the tangential feeding causes rotational liquid motion, hence a hollow core of low pressure inside the swirling chamber. The liquid exits the swirl atomizer in the form of a high-speed annular liquid film which develops and breaks

up into a conical spray.

It is asserted that four internal or external forces compete for disintegration and atomization of the swirl jet: centrifugal force due to vortical motion within the swirl chamber, aerodynamic force between the liquid sheet and interrupting gas, and surface tension. The cross-flow hinders the inertial motion of the liquid jet while it promotes the aerodynamic interaction. The effect of the cross-flow on the promotion of the atomization is better explained if the characteristics of the swirl spray with no presence of the cross-flow are known a priori. This isolates the influence of additional aerodynamic force due to the cross-flow interaction and thus provides better understanding of the swirl spray formation in view of the cross-flows. Geometric and operational parameters in Table 1 are repeatedly used.

In Fig. 4, the pressure swirl jets show the transition of spray patterns with increasing Weber number from 203 to 8,834 [21]. The spray profile is distinguished by five breakup regimes of (a) dribble, (b) distorted pencil, (c) onion, (f) tulip and (e) fully developed spray.

Each breakup regime is featured by three disintegration configurations of (a) rim, (b) wave, and (c) perforated sheet, and depends on the extent of the surface tension and Weber number [22]. In the rim mode, the surface tension enforces the free edge of a liquid sheet to contract into a thick rim and the liquids break up in the fashion of the free jet disintegration. Freshly formed drops continue inertial motion but are still tied up to the receding surface by thin threads. The jet breakup causes the formation of rows of large drops and numerous satellite drops. The disintegration is also caused by the amplification of a wave motion on the sheet. The liquid sheet is torn away with the size of a half or full wavelength before the leading edge is reached. Disintegrated liquid rapidly shrinks by the surface tension, but may experience the disintegration further due to aerodynamic interaction and the turbulence before a regular network of threads is formed. At higher Weber number, a perforated-sheet breakup occurs. Holes appear on the liquid sheet and are delineated by the rims thickened after the perforation. These holes grow rapidly in their size until the rims of adjacent holes coalesce and produce ligaments of irregular shape, and then the ligament eventually breaks up into drops.

Fig. 5 presents the contours of cross-sectional SMD (Sauter mean diameter, D_{32}) distributions at different injection velocities (Weber number). Axial location of the cross-section is 4 cm downstream from the nozzle tip and each grid size is 5mm. As stated, more than 5,000 drops were sampled to ensure a highly resolved SMD distribution with the confidence limit of 95%. Except the Weber number of 3,378 (Fig. 5(a)) in the case when the centrifugal motion is not strong enough to overwhelm the contracting surface tension, the breakup of all other swirl jets is in the fully turbulent flow regime. At all Weber numbers, larger drops are crowded in the vicinity of the liquid sheet and the drops get smaller toward either the spray core or the spray edge. This peculiar profile of the drop

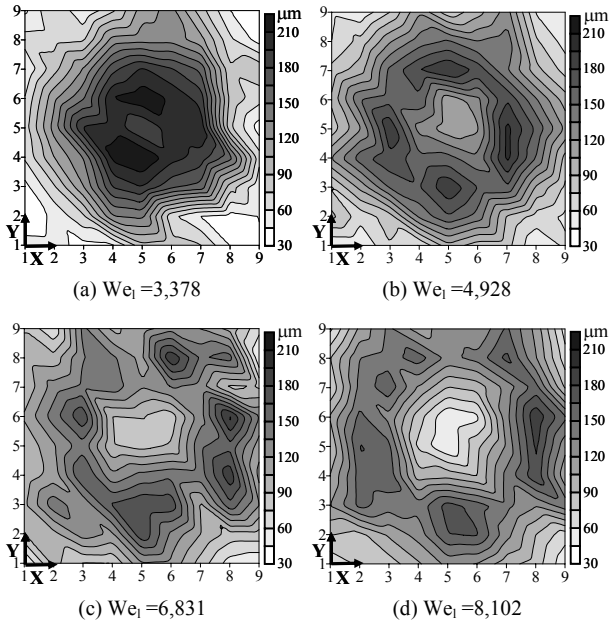

Fig. 5. SMD distribution on the cross-section at 4cm downward from the nozzle tip in still atmosphere (3,378< We$_l$<8,102).

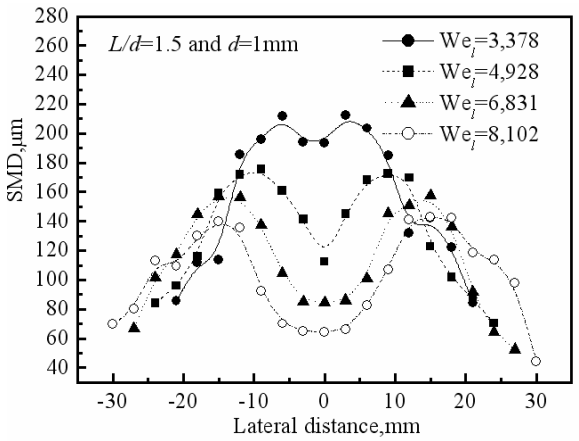

Fig. 6. SMD distribution along the horizontal centerline to the plane of swirl jets.

size distribution originates from the hollow-cone liquid projection. Enforced by centrifugal force, it becomes gradually thinner for continuity and disintegrates into smaller drops as the liquid cone stretches out [23]. As the Weber number increases from 4,928 (Fig. 5(b)) to 8,102 (Fig. 5(d)), the annular SMD distribution hence expands with increasing in the angular momentum.

Fig. 6 plots SMD variation into the radial direction at Weber numbers in the range from 3,378 to 8,102. As expected from Fig. 5, at all Weber numbers, SMD gets smaller symmetrically either into the spray core or outwards into the radial direction; its peak occurs at the location where the liquid sheet breaks up. With increasing Weber number, the aerodynamic interaction gives rise to Kelvin-Helmholtz waves on the liquid surface. The unstable waves are readily amplified. Growth rates of the

amplitude and the wave length depend on the relative velocity only. When the wave amplitudes arrive at certain limit, the sheet tends to breakdown at the crests and troughs in the magnitude of the half-wavelength. Since both the wavelength and the breakup length become shorter at higher injection velocities, the aerodynamic interaction evolves more intensively at this higher Weber number. Since the thickening rate of the liquid sheet at an instance of the sheet breakup is less than the rate of decrease in wavelength, the drop size diminishes as Weber number rises.

4.2 Breakup and spray formation in cross-flows

Snapshot pictures in Fig. 7 show how the cross-flow alters the breakup of the swirl jet at lower injection velocity of 3.9 m/s (We_l =0.25). Here the momentum ratio (q) varies within the range from 9 to 331. In Fig. 7 through Fig. 9, only lateral views of the jet breakup are shown for simplicity because the cross-flow exerts bending force onto the face (to the right of Fig. 7) of the liquid sheet. In Fig. 7, Weber number is so low at 0.25 that resultant liquid stream undergoes column breakup because of insufficient centrifugal forces enough to form the liquid sheet. This profile of the liquid stream projecting from the swirl injector mimics the liquid jet of a dribbled stage shown in Fig. 4(a). When the momentum ratio is 331 (Fig. 7(a)), the liquid column is deformed into the spherically protruding shape by the surface tension and then disintegrates into drops by the inertial force, and thereafter droplets spread by the centrifugal force. In this regime of lower Weber numbers, the liquid stream experiences Rayleigh-like breakup, a hydrodynamic instability caused by the surface tension. Symmetric dilatational waves due to the interaction of the liquid jet and surface tension occur across the liquid sheet [24]. If the wavelength of initial disturbance is greater than the minimum wavelength of the disturbance, the surface tension force tends to increase the disturbance and leads to the jet disintegration.

The uniform air-flows are blocked by traversing liquid stream and slowed down in order to redirect their streamlines for going around less mobile liquids. Reduction in the cross-flow momentum causes augmentation of the static pressure at the front of the liquid column. Resultant pressure drag causes bending of the liquid column. The lower the momentum ratio (higher gas Reynolds number) is, the larger the pressure difference is. The pressure force flattens the liquid column toward downstream and amplifies the aerodynamic waves, and the liquid column undergoes bag breakup (Fig. 7(c)). The geometry of the bag breakup is featured by a thin hollow bag attached to a thicker toroidal rim. In the lateral view, the liquid column is disintegrated into the loop-like structure at the node. The bag ruptures and then the toroidal rim. The former results in a large number of small fragments, whereas the latter a small number of large fragments. When the gas Reynolds number is further increased to 1,937 (q=9), the liquid column is more flattened and the secondary breakup is activated (Fig. 7(f)).

Fig. 8 exhibits the sprays at an intermediate Weber number of 0.81 with the momentum ratios varying in the range from 28

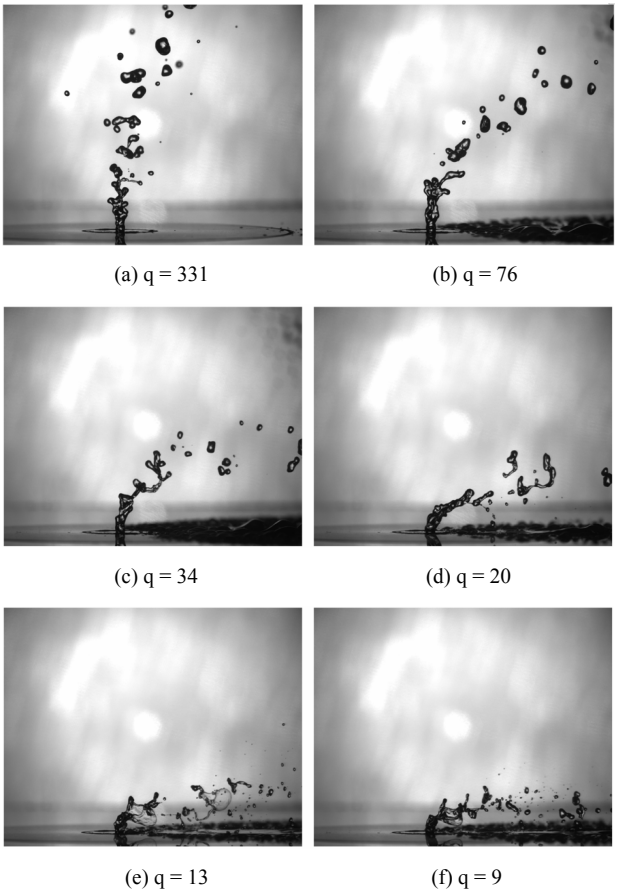

(a) q = 331 (b) q = 76

(c) q = 34 (d) q = 20

(e) q = 13 (f) q = 9

Fig. 7. Breakup of the swirl jet at lower Weber number (We_l =0.25) in momentum-ratio range from 9 to 331.

to 1,071. At the higher momentum ratio of 1,071 (Fig. 8(a)), the profile of the liquid stream projecting from the swirl injector mimics the liquid jet break up in an onion stage (Fig. 4(c)). The liquid stream accelerated into tangential and axial directions through helical passage within the swirl chamber stretches out while it forms a conical spray with a void in the spray core (Fig. 1). Radial velocity of the stretching liquid sheet rises in proportion to the Weber number (injection velocity); hence the liquid sheet stretches out and grows thinner for continuity as it proceeds downstream. But the hollow-conical liquid sheet tends to converge into a solid jet again. Henceforth the contracted liquid sheet is changed into ligaments and then it is disrupted into drops by Rayleigh jet breakup. The surface tension forces try to return the protuberance back to its original position, but the air experiences a local decrease in static pressure (corresponding to the local increase in velocity) that tends to expand the protuberance farther outward. This corresponds to the normal pattern of wind-induced instability, where surface tension forces oppose any movement of the interface from its initial plane and attempt to restore equilibrium, while the aerodynamic forces increase any deviation from the interface and thereby promote instability. Because of its widened contact surface, the liquid sheet is more apt to be disturbed by the cross-flows. After the formation of the liquid sheet, the surface

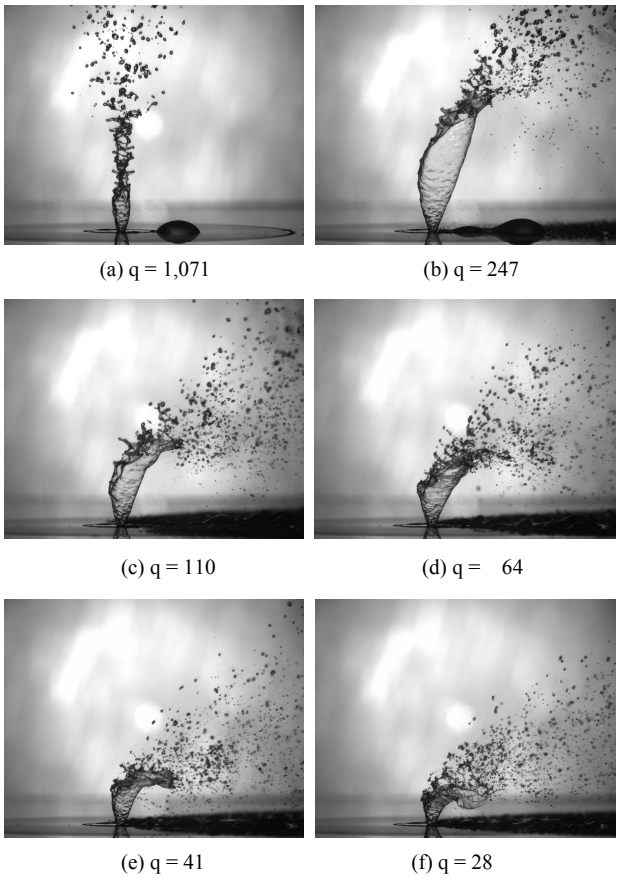

(a) q = 1,071 (b) q = 247

(c) q = 110 (d) q = 64

(e) q = 41 (f) q = 28

Fig. 8. Breakup of the swirl jet at intermediate Weber number (We_l =0.81) interacting with cross-flows in momentum-ratio range from 28 to 1,071.

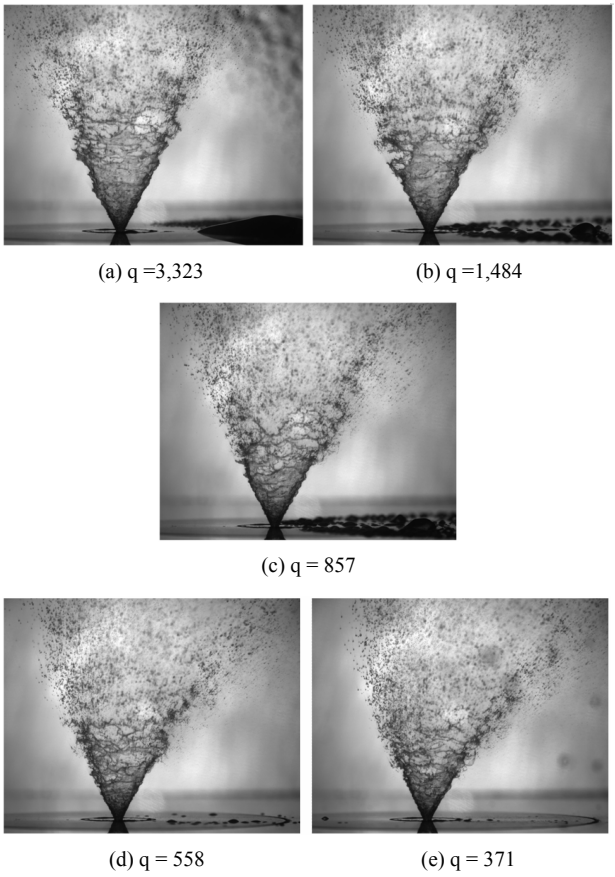

(a) q =3,323 (b) q =1,484

(c) q = 857

(d) q = 558 (e) q = 371

Fig. 9. Breakup of the swirl jet at high Weber number (We_l =10.89) interacting with cross-flows in momentum-ratio range from 371 to 3,323.

tension and the aerodynamic force compete. The liquid sheet is deformed and dispersed with increase in the cross-flow velocity [25, 26].

As momentum ratio decreases (Fig. 8(b)-8(f)), the viscous momentum loss of the cross-flows which turn around into the rear of the liquid sheet gives rise to the reduction of the static pressure. Consequently, the flow state and the extent of interaction differ due to the presence of the cross-flow. At the front, the aerodynamic interaction is activated in proportion to increasing in the cross-flow momentum. The front is directly exposed to the cross-flow and thus flattened and perturbed while it undergoes multimode breakup (bag/plume). Similar to the bag breakup, the bag is disintegrated and then the rim and the plume. The size spectrum of the liquid fragments is wide-banded. On the other hand, the liquid sheet stretches downstream at the rear because of the pressure drag. Surface interaction owing to freshly generated secondary flows is promoted; hence the liquid sheet is continuously eroded away and rapidly disintegrated. At very low momentum ratios (Fig. 8(e) and 8(f)), the rear of the liquid sheet is corrugated by waves of large amplitude and long wavelength and henceforth it forms a small number of large fragments that break up into smaller drops (sheet-thinning) [27].

Fig. 9 shows the spray images at high Weber number of 10.89 and momentum ratios from 371 to 3,323. At this high Weber number over 10, the hydrodynamic wave of relatively short wave length acts on the liquid sheet and gives rise to the surface wave of short wavelength across the entire liquid sheet. It disintegrates the liquid sheet into the ligament bands, and the ligaments are progressively disrupted into the drops by shear force. In addition, the perforation breakup mode is also observed owing to occurrence of strong turbulence in the liquid sheet. In perforated-sheet disintegration mode, the holes grow rapidly in their size until the rims of adjacent holes coalesce to produce ligaments of irregular shape that finally break up into drops. The drop sizes are broad-banded.

This profile of the liquid stream projecting from the swirl injector mimics the liquid jet of a fully developed spray shown in Fig. 4(f). Even at lower the momentum ratios of 558 and 371, the injected sprays are little bent by the pressure forces exerted by the cross-flows and exhibit the breakup pattern similar to the case of lower gas Reynolds number (Fig. 9(b) and 9(e)). Consequently, at higher Weber numbers, the spray dynamics weakly depends on the momentum ratio. It is well known that, in the case of the plane single jet interacting with strongly convective cross-flows, the momentum ratio is an essential parameter in order to estimate the macroscopic spray characteristics such as penetration extents. However, the swirl

sprays interacting with cross-flows exhibit distinctly different profiles in a narrow range of the momentum ratios (Fig. 8(b) and Fig. 9(e) q=247 and 371, respectively). Therefore, one must first have an understanding of the breakup process with the Weber number and momentum ratio. The growth of wave at the rear of the liquid sheet and the perforation which provides an additional breakup potential may be a plausible cause.

4.3 Cross-flow effects on the spray parameters

Macro and microscopic spray characteristics of the swirl sprays in low speed cross-flows were measured with emphasis on the cross-flow effects on the promotion of atomization and spray formation. The momentum carried by the cross-flow is converted into the static pressure which differs at the front and the rear of liquid sheet. Part of the static pressure is spent to bend the liquid jet toward the direction of cross-flow and the rest to disintegrate the liquids through multiple interaction passageways. Owing to an additional momentum transported by the cross-flow, the jet breakup is by and large activated. In Fig. 10, plots in the breakup lengths are presented in terms of inlet velocity of the cross-flow and Weber number. Here the breakup length is defined as the distance from the nozzle tip to the location where the liquid sheet is disconnected into ligament or droplet. Levels of aerodynamic and hydraulic interactions are estimated in terms of Weber number and the momentum ratio, respectively. Therefore, the occurrence of shorter breakup length is expected at higher cross-flow velocities at a fixed Weber number (Fig. 10(a) and Fig. 10(b)) or lower Weber numbers at a fixed momentum ratio (Fig. 10(c) and Fig. 10(d)). Fig. 10(a) and Fig. 10(b) show the breakup lengths decreasing with increasing cross-flow velocities at the front and the rear of the liquid sheet. As the Weber number rises, an annular liquid sheet projected from a swirl spray expands more due to augmented centrifugal forces concurrent with longer breakup length, but suddenly shrinks as Weber number is further increased over 2.49. This non-monotonic variation of the breakup length is relevant to the flow transient from laminar to turbulent jet. At higher gas Reynolds number (u_g=38) and lower Weber number in the laminar regime, the slight increase in the breakup length with increasing Weber numbers is due to the flattened liquid jets and sheets. In Fig. 10(c) and Fig. 10(d), formation of the laminar swirl jet with Weber number of 0.25 is expected to mimic the plain jet disintegration in the first and the second wind breakup regime. At the front, the liquid sheet is more apt to be disturbed by interrupting cross-flows and consequently it disintegrates into ligaments and drops due to the surface waves (Kelvin-Helmholtz waves) generated on the liquid sheet. As the cross-flow velocity increases, the breakup length decreases due to the amplified surface waves. At the rear, it yields longer breakup length in accordance with increasing in the cross-flow velocity, but shrinks as the cross-flow velocity rises over 13 m/sec at which the front surface ruptures and the cross-flow directly exerts the force to the rear surface. When the Weber number rises over

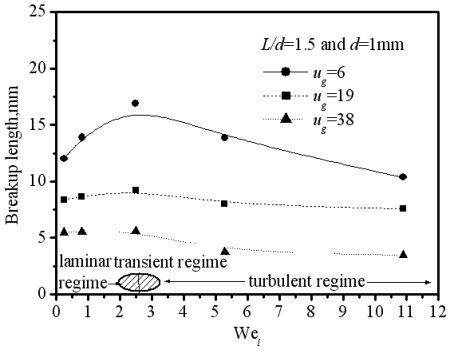

(a) Breakup length at the front liquid sheet versus jet Weber number

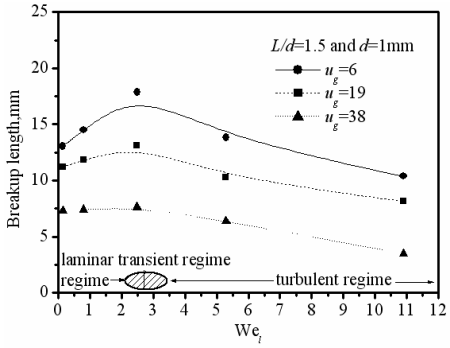

(b) Breakup length at the rear liquid sheet versus jet Weber number

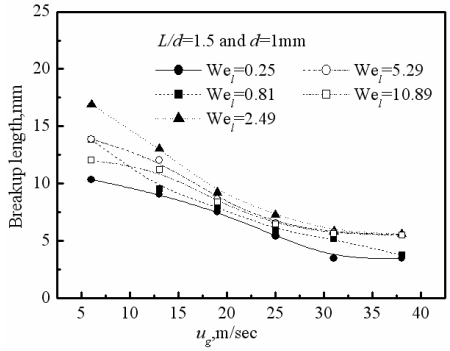

(c) Breakup length at the front liquid sheet versus cross-flow velocity

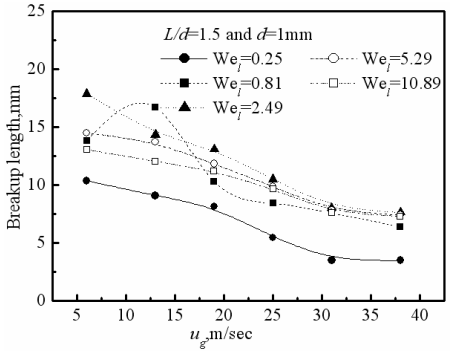

(d) Breakup length at the rear liquid sheet versus cross-flow velocity, cross-flow velocities for the rear liquid sheet (u_g)

Fig. 10. Effects of the injection and cross velocities on the breakup length.

2.49, the liquid jets enter into the turbulent flow regime. In the turbulent flow regime, the momentum transfer into the liquid

sheet is greatly promoted because the particles of fluids move irregularly, causing continuous exchange of momentum from one portion to another (i.e., turbulent shear stress due to the eddy structure). In addition, the turbulence causes a rugged surface which is more apt to be deformed by the aerodynamic drag by shearing cross-flows. Under these injection configurations, the turbulence tends to reduce the breakup length and promote atomization.

Penetration by a spray is estimated by the maximum distance which leading edge of the liquid sheet reaches, and its vertical component is frequently termed as the penetration height. The penetration height which limits the size of the inlet duct or a combustor is one of the essential geometrical design factors in conjunction with the breakup length. An excessive penetration height may cause wall-wetting and an uneven mixture-ratio distribution. Such non-uniformity lowers the thermal efficiency and often jeopardizes the system with a serious thermal compatibility problem. In Fig. 11, the penetration height consistently decreases with increasing in the cross-flow velocity. At fixed cross-flow velocity, the penetration height increases with Weber number. Similarly, at fixed injection velocity (constant Weber number), it decreases with increasing in the cross-flow velocity.

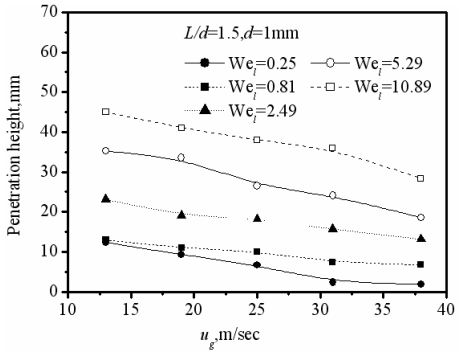

Fig. 11. Effect of the cross-flow velocity on the penetration heights at different jet Weber number.

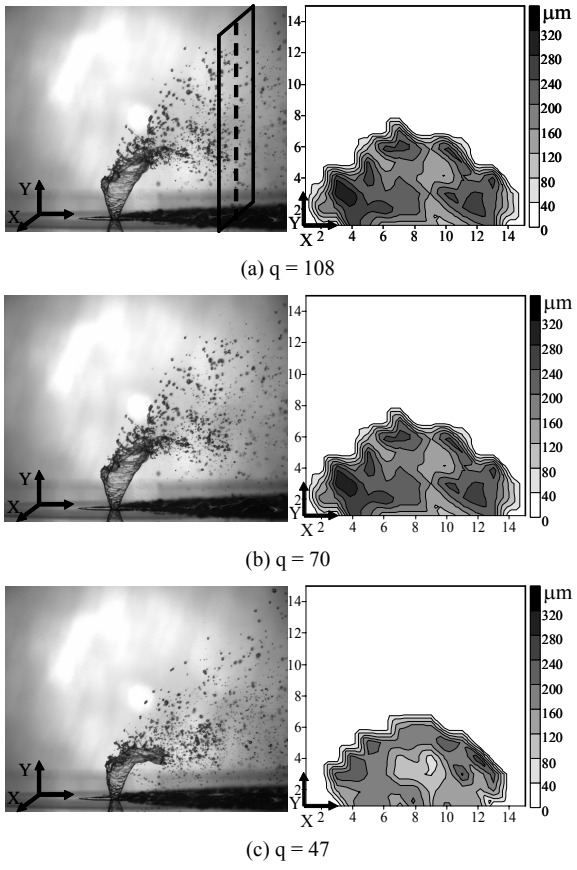

Fig. 12. Profiles of spray formation by the swirl jets (left) and cross-sectional iso-SMD lines (right) (We_l=1.37).

Fig. 12 shows lateral views of swirl spray (left) and cross-sectional SMD distribution (right). Each grid size is 1cm, and the momentum ratio is varied in the range from 47 to 108 with the Weber number fixed at 1.37. Comparing the left and right figures, the drop number density evolves with the axial location. The imaging was made on the cross-section at 7.5 cm downstream of the injection orifice. Thus the spray projecting upward is gravitationally bent down in proportion to the axial distance. The axial distance of 7.5 cm corresponds to the location where all primary and secondary breakup and spray formation is completed. This SMD profile is different from the annular distribution in the case of the still gases in Fig. 5.

5. Conclusions

Breakup and spray dynamics of swirl liquid jet introduced into a low-speed cross-flow were experimentally investigated. Macroscopic and microscopic spray parameters were examined in terms of the jet Weber number and the momentum ratio, and following conclusions are drawn.

At lower jet Weber numbers, the liquid stream undergoes Rayleigh jet breakup. At higher momentum ratios, the bag breakup occurs and tends to distort the liquid column into a loop-like structure. At intermediate jet Weber numbers, aerodynamic interaction and freshly formed secondary flows induce amplification of the surface waves and multi-mode breakup. The liquid sheet is continuously eroded from the surface and then disintegrates rapidly. At higher Weber numbers, the spray dynamics weakly depends on the momentum ratio and thus the spray profile is hardly altered by the cross-flows.

At all Weber numbers, larger drops are crowded in the vicinity of the liquid sheet and the drops become smaller toward either the spray core or the spray edge. The cross-flow promotes the jet breakup and renders a finer spray in the entire range of injection velocities. Its effect is more prominent at lower injection velocities.

References

[1] K. A. Sallam and H. M. Metwally et al., Deformation and surface waves properties of round non-turbulent liquid jets in gaseous cross-flow, *ASME Fluid Engineering Summer Con-*

ference,ASME Paper No. FEDSM2005-77469, Huston, TX, America, (2005) 19-23.
[2] S. J. Beresh and J. F. Henfling et al., Penetration of a transverse supersonic jet into a subsonic compressible cross-flow, *AIAA Journal*, 43 (2) (2005) 379-389.
[3] K. A. Sallam and C. L. Aalburg et al., Breakup of round non-turbulent liquid jets in gaseous cross-flows, *AIAA Journal*, 42 (12) (2004) 2529-2540.
[4] M. Y. Leong and V. G. McDonell et al., Effect of ambient pressure on an air-blast spray injected into a cross-flow, *J. Propul. Power*, 17 (5) (2001) 1076-1084.
[5] R. P. Fuller and P. K. Wu et al., Effects of injection angle on atomization of liquid jets in transverse airflow, *AIAA Journal*, 38 (1) (2000) 64-72.
[6] P. K. Wu and K. A. Kirkendall et al., Spray structures of liquid jets atomized in subsonic cross-flows, *J. Propul. Power*, 14 (2) (1998) 173-182.
[7] P. K. Wu and K. A. Kirkendall et al., Spray trajectories of liquid fuel jets in subsonic cross-flows, *7th international Conference on Liquid Atomization and Spray Systems*, Seoul, Korea, (1997).
[8] S. C. Li and K. Gebert, Spray characterization of high pressure gasoline fuel injectors with swirl and non-swirl nozzles, *California University*, San Diego, America (1998) SAE Technical Paper series.
[9] Z. Dai and G. M. Faeth et al., Temporal properties of secondary drop breakup in the multimode breakup regime, *Int. J. Multiphase Flow*, 24 (6) (1998) 889-912.
[10] G. I. Taylor, The boundary layer in the converging nozzle of a swirl atomizer, *Q. J. Mech. Appl. Math.*, 3 (2) (1950) 129-139.
[11] N. K. Rizk and A. H. Lefebvre, Internal flow characteristics of simplex swirl atomizer, *J. Propul. Power*, 1 (3) (1985) 193-199.
[12] N. K. Rizk and A. H. Lefebvre, Prediction of velocity coefficient and spray cone angle for simplex swirl atomizer, *Proc. of International Conference on Liquid Atomization and Spray Systems*, (1985).
[13] D. J. Kim and J. H. Im et al., Effects of ambient gas density on spray characteristics of swirling liquid sheets, *J. Propul. Power*, 23 (3) (2007) 603-611.
[14] D. J. Kim and P. G. Han et al, Effect of flow condition and geometry on flow characteristics of a swirl injector, *ILASS Americas, 16th Annual Conference on Liquid Atomization and Spray Systems*, Monterey, CA (2003).
[15] I-ping Chung and C. Presser, Fluid property effects on sheet disintegration of a simplex pressure swirl atomizer, *J. Propul. Power*, 17 (1) (2001) 212-216.
[16] J. L. Santolaya and L. A. Aisa et al., Experimental study of near-field flow structure in hollow cone pressure swirl spray, *J. Propul. Power*, 23 (2) (2007) 382-389.
[17] I. G. Bowen and G. P. Davies, "Report ICT 28," *Shell Research Ltd.*, London, UK, (1951).
[18] D. P. Schmidt, Idr. Nouar, P. K. Senecal, C. J. Rutland, J. K. Martin and R. D. Reitz, Pressure-swirl atomization in the near field, *SAE Technical Paper Series*, 1999-01-0496.
[19] P. K. Senecal, D. P. Schmidt, I. Nouar, C. J. Rutland, R.D Reitz and M. L. Corradini, Modeling high-speed viscous liquid sheet atomization, *Int. J. of Multiphase Flow*, 25 (1999) 1073-1097.
[20] A. H. Lefebvre, *Atomization and sprays*, Second Ed. Hemisphere, Philadelphia, USA, (1989) 30.
[21] A. H. Lefebvre, *Atomization and sprays*, Second Ed. Hemisphere, Philadelphia, USA, (1989) 112-116.
[22] R. P. Fraser and P. Eisenklam, Research into the performance of atomizers for liquids, *Imperial College of Chemical Engineering and Society*, 7 (1953) 52-68.
[23] M. S. M. R. El-Shanawany and A. H. Lefebvre, Airblast atomization: the effect of linear scale on mean drop size, *J. Energy*, 4 (4) (1980) 184-189.
[24] R. D. Reitz, Atomization and other breakup regimes of a liquid jet, Ph. D. Thesis, *Princeton University*, NJ, (1978).
[25] J. L. York and H. F. Stubbs et al., The mechanism of disintegration of liquid sheets, *Trans. ASME*, 75 (1953) 1279-1286.
[26] S. S. Lee, W. H. Kim and W. S. Yoon, Formation of Impinging Spray in Low Speed Cross Flow, *J. Mech. Sci. Technol.,* 23 (6) (2009) 1680-1692.
[27] D. R. Gulidenbecher, C. Lopez-Rivera and P. E. Sojka, Secondary atomization, *J. Exp. Fluids*, 46 (3) (2009) 371-402.

Woong-Sup Yoon is a Professor in the School of Mechanical Engineering at Yonsei University. His current research interests are in wave instabilities, unusual spray formation, emission control, and propulsion system modeling. He received a BS degree from the Department of Mechanical Engineering, Yonsei University, in 1985; an MS degree from the Department of Mechanical Engineering, University of Missouri-Rolla, in 1989; and a Ph.D degree from the Department of Mechanical and Aerospace Engineering, the Unversity of Alabama in Huntsville, in 1992.

Sang-seung Lee received his B.S. degree in Weapons Engineering from Korea Military Academy, Korea, in 2002. He then received his M.S. degrees from Yonsei University, in 2006. Mr. Lee is currently a Lecturer at the School of Weapons Engineering at Korea Military Academy in Seoul, Korea. He serves as an Editor of the Journal of Mechanical Science and Technology. Mr. Lee's research interests include Ramjet, Atomization of injector.

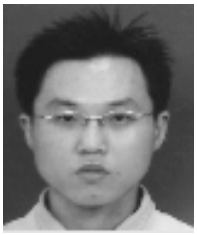

Won-ho Kim received his B.S. degree in Mechanical Engineering from Yonsei University, Korea, in 2003. Mr. Kim has then gone on to do graduate work at the Ph.D in the School of Mechanical Engineering at Yonsei University in Seoul, Korea. Mr. Kim's research interests include Atomization of 2phase flow and Dust collection efficiency.